Liquid temperature dependence of kinetic boundary condition at vapor–liquid interface

Misaki Kon[1], Kazumichi Kobayashi[1,*], Masao Watanabe[1]

Division of Mechanical and Space Engineering, Faculty of Engineering, Hokkaido University, Kita 13 Nishi 8, Kita-ku, Sapporo, Hokkaido 060-8628, Japan

Abstract

For the accurate description of heat and mass transfer through a vapor–liquid interface, the appropriate modeling of the interface during nonequilibrium phase change (net evaporation/condensation) is a crucial issue. The aim of this study is to propose a microscopic interfacial model which should be imposed at the interface as the kinetic boundary condition for the Boltzmann equation. In this study, we constructed the kinetic boundary condition for monoatomic molecules over a wide range of liquid temperature based on mean field kinetic theory, and we validated the accuracy of the constructed kinetic boundary condition by solving the boundary value problem of the Boltzmann equation. These results showed that we can impose the kinetic boundary condition at the interface by simply specifying liquid temperature and simulate the complex vapor–liquid two-phase flow induced by net evaporation/condensation. Furthermore, we applied the constructed kinetic boundary condition to the boundary condition for the fluid-dynamic-type equations. This application enables us to deal with a large spatio-temporal scale of the interfacial dynamics in the vapor–liquid two-phase system with net evaporation/condensation.

Keywords: kinetic boundary condition, evaporation and condensation, vapor–liquid interface, kinetic theory of gases

1. Introduction

Heat and mass transfer through a vapor–liquid interface induced by nonequilibrium phase change (net evaporation/condensation) plays an important role in dynamics of the vapor–liquid two-phase flows, such as Leidenfrost effect[1, 2, 3] and cavitation bubble collapse [4, 5, 6]. In recent years, furthermore, with the progression of micro/nanofluidic devices, the precise investigation of transport phenomena during net evaporation/condensation has been required[7].

* *Email addresses:* konmi@eng.hokudai.ac.jp (Misaki Kon), kobakazu@eng.hokudai.ac.jp (Kazumichi Kobayashi), masao.watanabe@eng.hokudai.ac.jp (Masao Watanabe)

Since net evaporation/condensation originates from the motion of molecules in the vicinity of the interface, the vapor in contact with the interface is in nonequilibrium in which the conventional continuum description is not appropriate, and the analysis of the Boltzmann equation based on kinetic theory of gases (molecular gas dynamics) is essential[8]. The Boltzmann equation governs the spatio-temporal development of the molecular velocity distribution function, $f(\boldsymbol{x}, \boldsymbol{\xi}, t)$, defined as $\mathrm{d}N = (1/m) f(\boldsymbol{x}, \boldsymbol{\xi}, t) \mathrm{d}\boldsymbol{x}\mathrm{d}\boldsymbol{\xi}$, where $\boldsymbol{x} = (x, y, z)$ is position, $\boldsymbol{\xi} = (\xi_x, \xi_y, \xi_z)$ is molecular velocity, $\mathrm{d}\boldsymbol{x}\mathrm{d}\boldsymbol{\xi} = \mathrm{d}x\mathrm{d}y\mathrm{d}z\mathrm{d}\xi_x\mathrm{d}\xi_y\mathrm{d}\xi_z$ is an infinitesimal volume element in the six-dimensional phase space, $\mathrm{d}N$ is the number of molecules in $\mathrm{d}\boldsymbol{x}\mathrm{d}\boldsymbol{\xi}$, and m is the mass of a molecule. Once the velocity distribution function f is obtained as the solution of the Boltzmann equation, the macroscopic variables, such as density, velocity, and temperature, are obtained from its moments

$$\rho = \int_{-\infty}^{\infty} f \mathrm{d}\boldsymbol{\xi}, \quad v_i = \frac{1}{\rho} \int_{-\infty}^{\infty} \xi_i f \mathrm{d}\boldsymbol{\xi}, \quad T = \frac{1}{3\rho R} \int_{-\infty}^{\infty} (\xi_i - v_i)^2 f \mathrm{d}\boldsymbol{\xi}, \tag{1}$$

where ρ is density, $v_i = (v_x, v_y, v_z)$ is velocity, T is temperature, R is the gas constant and $\int_{-\infty}^{\infty} \mathrm{d}\boldsymbol{\xi} = \int_{-\infty}^{\infty} \mathrm{d}\xi_x \int_{-\infty}^{\infty} \mathrm{d}\xi_y \int_{-\infty}^{\infty} \mathrm{d}\xi_z$.

In this analysis, we have to specify a molecular velocity distribution function composed of molecules outgoing from the liquid into the vapor phase, f_{out}, which should be imposed at the interface as the kinetic boundary condition (KBC) for the Boltzmann equation. Since it has been found that the KBC significantly affects the macroscopic variables obtained from Eq. (1)[8, 9] during net evaporation and condensation, the proper specification of the KBC at the interface is critical. One of the most conventional forms of the KBC is shown as follows:

$$f_{\mathrm{out}} = \left[\alpha_{\mathrm{e}} \rho^*(T_{\mathrm{L}}) + (1 - \alpha_{\mathrm{c}})\sigma\right] \hat{f}, \quad \xi_z > 0, \tag{2}$$

where ρ^* is the saturated vapor density, α_{e} and α_{c} are evaporation and condensation coefficients, respectively, ξ_z is the molecular velocity in the direction normal to the interface; $\xi_z > 0$ denotes the direction of molecular velocity outgoing from the liquid into the vapor phase, and $\hat{f}$ is a normalized molecular velocity distribution function; the normalized Maxwellian distribution at liquid temperature, T_{L},

$$\hat{f} = \frac{1}{(\sqrt{2\pi R T_{\mathrm{L}}})^3} \exp\left(-\frac{\xi_i^2}{2RT_{\mathrm{L}}}\right) \tag{3}$$

is assumed conventionally. σ is related to a molecular velocity distribution function composed of molecules colliding onto the liquid from the vapor phase ($\xi_z < 0$), f_{coll}. Its definition is

$$\sigma \sqrt{\frac{RT_{\mathrm{L}}}{2\pi}} = -\int_{\xi_z < 0} \xi_z f_{\mathrm{coll}} \mathrm{d}\boldsymbol{\xi} = J_{\mathrm{coll}}, \tag{4}$$

where J_{coll} is the molecular mass flux colliding onto the liquid from the vapor phase and $\int_{\xi_z<0} \mathrm{d}\boldsymbol{\xi} = \int_{-\infty}^{\infty} \mathrm{d}\xi_x \int_{-\infty}^{\infty} \mathrm{d}\xi_y \int_{-\infty}^{0} \mathrm{d}\xi_z$. f_{coll} at each time is obtained by solving the initial boundary value problem of the Boltzmann equation[8]; σ has a unit of density and is equal to ρ^* in the vapor–liquid equilibrium.

One of the most important issues in the construction of the KBC during net evaporation/condensation lies in the determination of the evaporation coefficient $\alpha_{\rm e}$ and the condensation coefficient $\alpha_{\rm c}$. As for the definitions of $\alpha_{\rm e}$ and $\alpha_{\rm c}$, some different models were proposed[10, 11, 12, 13, 14]. We adopt the following definitions of $\alpha_{\rm e}$ and $\alpha_{\rm c}$ as a widely-used model[12, 15, 16, 17, 18, 19, 20].

$$\alpha_{\rm e} = \frac{J_{\rm evap}}{J^*_{\rm out}}, \quad \alpha_{\rm c} = \frac{J_{\rm cond}}{J_{\rm coll}}, \tag{5}$$

where $J_{\rm evap}$ is evaporation molecular mass flux, $J_{\rm cond}$ is condensation molecular mass flux, and $J_{\rm out}$ is molecular mass flux outgoing from the liquid into the vapor phase; star (*) superscripts denote quantities at the vapor–liquid equilibrium and $J^*_{\rm out} = J^*_{\rm coll} = \rho^* \sqrt{(RT_{\rm L}/2\pi)}$. The relations of each molecular mass flux are as follows:

$$J_{\rm out} = J_{\rm evap} + J_{\rm ref}, \quad J_{\rm coll} = J_{\rm cond} + J_{\rm ref}, \tag{6}$$

where $J_{\rm ref}$ is molecular mass flux reflecting to the vapor phase (reflection molecular mass flux). The next task is to distinguish between $J_{\rm evap}$ and $J_{\rm ref}$ to estimate these molecular mass fluxes and then to determine $\alpha_{\rm e}$ and $\alpha_{\rm c}$.

In the vapor–liquid equilibrium, $\alpha_{\rm e}$ is equal to $\alpha_{\rm c}$ from the definition of Eq. (5), and that is confirmed based on molecular dynamics[12, 17, 18]. On the other hand, during net evaporation/condensation, several studies to determine $\alpha_{\rm e}$ and $\alpha_{\rm c}$ based on molecular dynamics have been proposed to date[15, 16, 19, 20]. For instance, Ishiyama *et al.*[19, 20] proposed a concept of *spontaneous evaporation* to avoid the ambiguities of assigning $J_{\rm evap}$ and $J_{\rm ref}$. They showed that $\alpha_{\rm e}$ and $\alpha_{\rm c}$ for monoatomic (argon) molecules take almost the same value during net evaporation/condensation. Meland *et al.*[15] distinguished these molecular mass fluxes by using *interphase boundary* and pointed out that $\alpha_{\rm e}$ and $\alpha_{\rm c}$ for monoatomic (argon) molecules vary with the increase in the Mach number of vapor far from the interface. Kryukov *et al.*[16] also found the increase in $\alpha_{\rm c}$ by accounting for monoatomic (argon and helium) molecules.

Neither $\alpha_{\rm e}$ nor $\alpha_{\rm c}$ has been indisputably determined after all, even though each of different coefficients had been derived from the same definition (Eq. (5)) with the use of simple monoatomic molecules. In other words, the distinction between $J_{\rm evap}$ and $J_{\rm ref}$ has still remained ambiguity. Furthermore, these studies[15, 16, 19, 20] investigated only a few cases of liquid temperature. It would be advantageous that the molecular dynamics simulations can deal with practical monoatomic and polyatomic molecules; however, it is extremely hard to conduct a systematic investigation of the KBC in consideration of the liquid temperature dependence because of its high computational cost.

In contrast to these studies, the authors[21] have proposed a novel method of determining the KBC for the monoatomic (hard-sphere) molecules based on mean field kinetic theory[22, 23]. This method can construct the KBC without distinguishing each molecular mass flux. The constructed KBC can describe accurate macroscopic variables, such as vapor density, velocity, and temperature, in the case of liquid temperature near the triple point.

Furthermore, incorporating mean field kinetic theory, we can succeed to reduce the computational cost compared with the molecular dynamics simulations. However, any dependence of the KBC constructed by this method with liquid temperature has yet to be explored.

In this study, we conduct a systematic investigation of the KBC during net evaporation/condensation by considering the liquid temperature dependence. First, we construct the KBC during net evaporation/condensation by using this method over a wide range of liquid temperatures (Sec. 3.2). Then, we validate the accuracy of the constructed KBC by solving the boundary value problem of the Boltzmann equation (Sec. 3.3). Finally, we comment on the application of the constructed KBC to the boundary condition for the fluid-dynamic-type equations (Sec. 3.4).

2. Method

2.1. Numerical simulation of the Enskog–Vlasov equation

In this study, we utilize a DSMC-based numerical scheme employing the Enskog–Vlasov equation to construct the KBC. This numerical scheme provides the reasonable description of the vapor–liquid two-phase flow.

The Enskog–Vlasov equation[22, 23] is a kinetic equation based on mean field kinetic theory, which describes the hard-sphere fluid interaction by Sutherland potential, $\phi(r)$, defined as

$$\phi(r) = \begin{cases} +\infty & (r < a) \\ -\phi_a \left(\frac{r}{a}\right)^{-\gamma} & (r \geq a), \end{cases} \tag{7}$$

where r is intermolecular distance, a is a molecular diameter, ϕ_a and γ are constants; γ is set as six to follow the attractive tail of the 12–6 Lennard–Jones intermolecular potential. In terms of a one-particle velocity distribution function, the Enskog–Vlasov equation is expressed as

$$\frac{\partial f}{\partial t} + \xi_i \frac{\partial f}{\partial x_i} + \frac{F_i(x_i, t)}{m} \frac{\partial f}{\partial \xi_i} = C_E, \tag{8}$$

$$\begin{aligned} C_E = \quad & a^2 \int \{Y[n(x_i + \frac{a}{2}K_i, t)] f(x_i + aK_i, \xi'_{1i}, t) f(x_i, \xi'_i, t) - Y[n(x_i - \frac{a}{2}K_i, t)] \\ & \times f(x_i - aK_i, \xi_{1i}, t) f(x_i, \xi_i, t)\} H(\xi_{ri} K_i)(\xi_{ri} K_i) \mathrm{d}\boldsymbol{\xi}_1 \mathrm{d}^2 \boldsymbol{K}, \end{aligned}$$

where t is time, x_i is position (x, y, and z), Y is a pair correlation function, n is number density, K_i is the unit vector defined as $K_i = (x_{1i} - x_i)/(\|x_{1i} - x_i\|)$, H is the Heaviside function, ξ_i and ξ_{1i} denote the molecular velocity of two colliding molecules; prime ($\prime$) superscripts denote quantities of post-collisional molecules, $\xi_{\mathrm{r}i}$ denotes the relative velocity $\xi_{\mathrm{r}i} = \xi_i - \xi_{1i}$, and F_i is a self-consistent force field determined from Eq. (7)[24]

$$F_i(x_i, t) = \int_{\|x_{1i} - x_i\| > a} \frac{\mathrm{d}\phi}{\mathrm{d}r} \frac{x_{1i} - x_i}{\|x_{1i} - x_i\|} n(x_{1i}, t) \mathrm{d}x_{1i}, \tag{9}$$

where x_i and x_{1i} denote the molecular position of two colliding molecules.

As for the equation of state for hard-sphere molecules, we utilized Carnahan and Stirling approximation[25]. According to this equation of state, the critical temperature of hard-sphere molecules is given as follows[24]:

$$T_{\mathrm{c}} = 0.094329 \frac{4\gamma}{\gamma - 3} \frac{\phi_a}{k}, \tag{10}$$

where k is the Boltzmann constant. We estimate the saturated vapor density, ρ^*, of hard-sphere molecules from the Clausius–Clapeyron equation obtained from the vapor–liquid equilibrium simulation[21]

$$\frac{\rho^*(T_{\mathrm{L}})}{\rho_{\mathrm{c}}} = 79.72 \frac{T_{\mathrm{c}}}{T_{\mathrm{L}}} \exp\left(-5.279 \frac{T_{\mathrm{c}}}{T_{\mathrm{L}}}\right), \tag{11}$$

where ρ_{c} is critical density.

To solve the Enskog–Vlasov equation, we utilized a DSMC-based numerical scheme (EV-DSMC)[24, 26]; the DSMC method is one of the particle schemes for solving the kinetic equation[27, 28]. The great advantage of using this method is its capability to deal with the larger number of particles than the molecular dynamics simulations[29], which enable us to obtain precise macroscopic variables in the vapor–liquid two-phase flow. Furthermore, several studies have confirmed that macroscopic variables obtained from the EV-DSMC simulation show similar tendencies with those obtained from the molecular dynamics simulation for monoatomic molecules[21, 24, 30, 31].

2.2. Simulation system

We considered a one-dimensional physical space (z-direction) and three-dimensional molecular velocity space in the system that is composed of hard-sphere vapor and its condensed phase (liquid). Note that to assume a one-dimensional physical space, the vapor–liquid interface has to be planar; the interface having a curvature should be considered as a two- or three-dimensional physical space. On the other hand, the characteristic length scale of evaporation/condensation is molecular diameter order. In this length scale, the vapor–liquid interface is approximately planar even though it has a curvature in the macroscopic scale.

Figure 1 (above) shows a schematic of the simulation system. Liquids at temperatures T_{Lh} and T_{Ll} ($T_{\mathrm{Lh}} > T_{\mathrm{Ll}}$) are confined to the regions around the left and right edges, respectively. The *kinetic boundary*, which is synonymous with the interface, is defined as the position where the KBC is imposed[21, 32]. The net mass flux, ρv_z, is induced in the direction outgoing from the liquid into the vapor phase at the kinetic boundary at T_{Lh} (net evaporation), and that is also induced in the direction colliding onto the liquid from the vapor phase at the kinetic boundary at T_{Ll} (net condensation). The relation of each molecular mass flux (Eq. (6)) in the simulation setting of this study is shown in the enlarged views of Fig. 1 (above). ρv_z is obtained as the difference between J_{out} and J_{coll} at each kinetic boundary. Note that net evaporation and condensation never occur simultaneously at the same kinetic boundary, whereas evaporation, reflection and condensation in a sense of molecular motions always occur at the same kinetic boundary.

Figure 1 (below) shows the density field and the various net fluxes obtained from the EV-DSMC simulation[24, 26]. A thin solid line is the density field, a bold solid line is the net mass flux in vapor, a dashed line is the net heat flux in vapor, and a dotted line is the net energy flux in vapor. T_{Lh} and T_{Ll} normalized by the critical temperature, T_{c}, are set as 0.68 and 0.60, respectively. In Fig. 1 (below), the high density regions around the left and right edges of the system are liquids, and the low density region around the center of the system is vapor. The smooth density transition layers are formed between vapor and each liquid. The fluxes in vapor are induced by the liquid temperature difference between T_{Lh} and T_{Ll}; the net mass and net energy fluxes in vapor take positive value in the z-direction, whereas the net heat flux in vapor takes negative value in the z-direction. This negative net heat flux is caused by the positive temperature gradient in vapor which is called *inverted temperature gradient*[8]. Note that several studies[33, 34, 35] have indicated that the negative mass flux is also caused by the inverted temperature gradient; we could not observe the negative mass flux because the occurrence of this phenomenon is highly unlikely indicated by the necessary and sufficient criteria[34, 35]. We further discuss the inverted temperature gradient and the negative heat flux in Sec. 3.1.

It is important that the net mass flux in vapor becomes uniform and constant as a consequence of steady net evaporation/condensation. To obtain steady net evaporation and condensation, we applied velocity-scaling and particle-shifting methods [21, 36]. The velocity-scaling method modifies molecular velocity in bulk liquid at each time step, keeping the constant liquid temperature, where the boundary of the bulk liquid is defined as $3a$ away from the center of the 10–90 thickness density transition layer, Z_{m}. The particle-shifting method modifies the position of molecules in whole simulation system, fixing the position of the kinetic boundary. To estimate ρv_z in the various cases of the degree of net evaporation and condensation, we varied the temperature difference of the two liquid slabs. Detailed settings of the liquid temperature differences are shown in Sec. 2.3.

2.3. Method of constructing the KBC

The method of constructing the KBC proposed in our recent study[21] is explained in the following. First, to eliminate J_{ref} in Eq. (6), we utilized the conservation law of the molecular mass flux at the kinetic boundary:

$$\rho v_z = J_{\mathrm{out}} - J_{\mathrm{coll}} = (J_{\mathrm{evap}} + J_{\mathrm{ref}}) - (J_{\mathrm{cond}} + J_{\mathrm{ref}}) = J_{\mathrm{evap}} - J_{\mathrm{cond}}. \tag{12}$$

If we assume the normalized velocity distribution function $\hat{f}$ in Eq. (2) to be the normalized Maxwellian distribution (Eq. (3)), the above equation can be rewritten as

$$\rho v_z = \left[\alpha_{\mathrm{e}}\rho^*(T_{\mathrm{L}}) - \alpha_{\mathrm{c}}\sigma\right]\sqrt{\frac{RT_{\mathrm{L}}}{2\pi}}. \tag{13}$$

Note that there has been some arguments about the assumption of the normalized Maxwellian distribution during stronger net evaporation/condensation[19, 20, 30]; hence, in our recent study, we examined the applicability of the above assumption over a wide range of liquid temperature[21, 32].

Second, we rewrote the KBC (Eq. (2)) by using the net mass flux ρv_z. Substitution of Eq. (13) in Eq. (2) leads to

$$f_{\mathrm{out}} = \frac{\left[\rho v_z \sqrt{\frac{2\pi}{RT_{\mathrm{L}}}} + \sigma\right]}{(\sqrt{2\pi RT_{\mathrm{L}}})^3} \exp\left(-\frac{\xi_i^2}{2RT_{\mathrm{L}}}\right), \quad \text{for } \xi_z > 0. \tag{14}$$

If ρv_z is uniquely specified, σ is estimated as a part of the solution of the Boltzmann equation by using Eq. (4).

Third, to estimate ρv_z in the various cases of the degree of net evaporation and condensation, we simulated the system of two liquid slabs at different temperatures as explained in Sec. 2.2. The formulated mass flux relations can be obtained by using the procedure proposed in our recent study[21]. We set the reference liquid temperature normalized by its critical value, $T_{\mathrm{L}}/T_{\mathrm{c}}$, as 0.60; this temperature is near the triple point temperature of argon molecules (83.8 K). As a result of our recent study, the mass flux relation at the kinetic boundary during net evaporation is as follows:

$$\frac{\rho v_z}{J^*_{\mathrm{out}}} = 0.871\left(1 - \frac{J_{\mathrm{coll}}}{J^*_{\mathrm{coll}}}\right) = 0.871\left(1 - \frac{\sigma}{\rho^*(T_{\mathrm{L}})}\right), \tag{15}$$

and that for net condensation is as follows:

$$\frac{\rho v_z}{J^*_{\mathrm{out}}} = 0.928\left(1 - \frac{\sigma}{\rho^*(T_{\mathrm{L}})}\right). \tag{16}$$

Each equation was constructed by using the linear regression analysis; the coefficient of determination, R^2, in this linear regression analysis was more than 0.999. Here, we defined the ratio of J_{coll} to J^*_{coll} as the index of the degree of net evaporation and condensation at the kinetic boundary; $J_{\mathrm{coll}}/J^*_{\mathrm{coll}} = \sigma/\rho^*$ in the vapor–liquid equilibrium is unity, while that in net evaporation and condensation are smaller and larger than unity, respectively. From this linear regression analysis, we confirmed that a linear mass flux relation indeed exists at $T_{\mathrm{L}}/T_{\mathrm{c}} = 0.60$.

Finally, to specify the KBCs at the kinetic boundaries during net evaporation and condensation, we substitute the linear mass flux relation (Eqs. (15) or (16)) to the KBC rewritten by ρv_z (Eq. (14)). In addition, when J_{coll} in Eq. (15) is set as zero, α_{e} according to the concept of spontaneous evaporation[12, 19] can be obtained as

$$\alpha_{\mathrm{e}} = 0.871. \tag{17}$$

Furthermore, with the use of Eqs. (15) and (17), α_{c} at the kinetic boundary during net evaporation is

$$\alpha_{\mathrm{c}} = \alpha_{\mathrm{e}} = 0.871. \tag{18}$$

In the same way, with the use of Eqs. (16) and (17), α_{c} at the kinetic boundary during net condensation is

$$\alpha_{\mathrm{c}} = \frac{\rho^*(T_{\mathrm{L}})}{\sigma}(\alpha_{\mathrm{e}} - 0.928) + 0.928, \tag{19}$$

These results showed that in the case of $T_{\rm L}/T_{\rm c} = 0.60$, $\alpha_{\rm e}$ and $\alpha_{\rm c}$ are identical and constant when the kinecit boudary is in net evaporation, on the other hand, $\alpha_{\rm c}$ increases with the increase in σ/ρ^* when that is in net condensation.

It is the most striking finding in our recent study[21] that ρv_z is well described as a linear function of σ/ρ^*, but it is not obvious that the existence of this linear mass flux relation at other liquid temperature. Thus, to construct the KBCs by using this method in consideration of the liquid temperature dependence, we have to confirm the existence of the linear mass flux relation at a given liquid temperature. Hereafter, for more general expression, we replace 0.871 and 0.928 in Eqs. (15) and (16) as $\beta_{\rm ne}$ and $\beta_{\rm nc}$, respectively. Obviously, the existence of the linear mass flux relation indicates that $\beta_{\rm ne}$ and $\beta_{\rm nc}$ are constants and depend only on liquid temperature. In this study, we formulate the mass flux relation between ρv_z and σ/ρ^* over a wide range of liquid temperature and then construct the KBC in consideration of the liquid temperature dependence.

As was mentioned, we varied the temperature differences of the two liquid slabs to estimate ρv_z in the various cases of σ/ρ^*; one of the liquid temperatures is fixed as *reference liquid temperature* $T_{\rm L}$, and the other liquid temperature is varied. We set the normalized reference liquid temperature $T_{\rm L}/T_{\rm c}$ as 0.60, 0.62, 0.64, 0.66, 0.68, 0.70, and 0.72. For instance, in the case of $T_{\rm L}/T_{\rm c} = 0.64$, $T_{\rm Ll}/T_{\rm c}$ is varied in the range of 0.56–0.63 with the increments of 0.01 if $T_{\rm Lh}/T_{\rm c}$ is fixed to 0.64 (net evaporation cases), while $T_{\rm Lh}/T_{\rm c}$ is varied in the range of 0.65–0.80 with the increments of 0.01 if $T_{\rm Ll}/T_{\rm c}$ is fixed to 0.64 (net condensation cases). In this manner, we performed the numerical simulations in 160 cases of the liquid temperature differences (Tables 1–7). The cell size, $\Delta z/a$, and the time-step size, $\Delta t/(a/\sqrt{2RT_{\rm c}})$, are set as 0.2 and 0.001, respectively.

3. Results and discussion

3.1. Macroscopic variables obtained from the EV-DSMC simulations

Figure 2 shows the density, velocity, and temperature fields obtained from the EV-DSMC simulation in the cases of the normalized reference liquid temperature $T_{\rm L}/T_{\rm c} = 0.60$ and 0.64; typical examples of the kinetic boundary at the reference liquid temperature during weak net condensation (Fig. 2(a) and (c)) with the small liquid temperature difference and that during strong net condensation (Fig. 2(b) and (d)) with the large liquid temperature difference are presented.

In each case of Fig. 2, the high density regions around the left and right edges of the system are liquids, and the low density region around the center of the system is vapor. The smooth density transition layers are formed between vapor and each liquid. As can be seen, a positive vapor velocity in the z-direction is induced by net evaporation/condensation in all cases. We found that the vapor velocity increases with the increase in the liquid temperature difference in the both cases of the normalized reference liquid temperature. Note that temperature at the kinetic boundary differs from that of bulk liquid, which is called *temperature jump* [13, 14, 15, 19, 37, 38, 39]. As shown in Fig. 2, the temperature jump increases with the increase in the liquid temperature difference in the both cases of the normalized reference liquid temperature; this increase in the temperature jump is

related to the increase in the velocity in the direction normal to the kinetic boundary[40]. Furthermore, in this system consisting of two liquid slabs at different temperatures, well-known characteristic phenomenon *inverted temperature gradient*[8, 41, 42, 43, 44] occurs in the bulk vapor as a consequence of the temperature jump. We verified the occurrence of the inverted temperature gradient by using the EV-DSMC simulation. As can be seen in enlarged views of Fig. 2, the temperature gradient at the center of vapor becomes positive in all cases. As a consequence of this inverted temperature gradient, the direction of the net heat flux in vapor is negative as shown in Fig. 1. Several studies[36, 45, 46] have also verified the inverted temperature gradient by using experimental and molecular dynamics-based approaches; Hermans and Beenakker[44] have proved that the inverted temperature gradient does not violate the second law of thermodynamics.

3.2. Formulation of the mass flux relation and construction of the KBC

Figure 3 shows the mass flux relation between the net mass flux ρv_z and the degree of net evaporation/condensation σ/ρ^*, at the kinetic boundary of each reference liquid temperature. In the discussion given below, for convenience, we set $\rho v_z > 0$ and $\rho v_z < 0$ at the kinetic boundary during net evaporation and net condensation, respectively (see Fig. 3). Each closed circle is obtained from the EV-DSMC simulation, and each solid line is obtained from the linear regression analysis; the coefficients of determination during net evaporation, R^2_{ne}, and net condensation, R^2_{nc}, at each reference liquid temperature are shown in Fig. 3. It should be emphasized that each closed circle in Fig. 3 corresponds to each case of the liquid temperature difference shown in Table 1–7. When the liquid temperature difference becomes larger, the deviation of σ/ρ^* from unity increases because of stronger net evaporation/condensation. As was mentioned in Sec. 2.3, several studies[19, 20, 30] have been proposed that $\hat{f}$ in the KBC deviate from the normalized Maxwellian distribution during stronger net evaporation/condensation. In our recent study[21, 32], we confirmed that this deviation becomes prominent with the increase in σ/ρ^*. We also determined that the range of σ/ρ^* in which $\hat{f}$ can be assumed to be the normalized Maxwellian distribution is from 0.5 to 2.3. Thus, the linear regression analysis can be applied in this range of σ/ρ^*. The detailed values of ρv_z and σ/ρ^* in all 160 cases are shown in Tables 1–7.

Figure 3 clearly shows that a linear relation between ρv_z and σ/ρ^* is obtained at each liquid temperature. In other words, since the slopes β_{ne} and β_{nc} are constant, we succeeded to confirm that these parameters are constant at each liquid temperature. The values of β_{ne} and β_{nc} are shown in Tables 1–7, and a relation between these parameters and liquid temperature are shown in Fig. 4. As can be observed, β_{ne} and β_{nc} decrease with the increase in liquid temperature, and β_{nc} is larger than β_{ne} at each liquid temperature. With the use of these results, we can rewritten Eqs. (15) and (16) as

$$\frac{\rho v_z}{J^*_{\mathrm{out}}} = \beta_{\mathrm{ne}}(T_{\mathrm{L}}) \left(1 - \frac{\sigma}{\rho^*(T_{\mathrm{L}})} \right), \tag{20}$$

$$\frac{\rho v_z}{J^*_{\mathrm{out}}} = \beta_{\mathrm{nc}}(T_{\mathrm{L}}) \left(1 - \frac{\sigma}{\rho^*(T_{\mathrm{L}})} \right), \tag{21}$$

Above equations showed that the change of ρv_z with the increase in σ/ρ^* during net condensation is larger than that for net evaporation. Note that with the use of Eqs. (20) and (21), we can derive general expressions of Eqs. (17)–(19); that is the relations between the evaporation coefficient α_e and the condensation coefficient α_c defined by Eq. (5) and β_ne or β_nc. A general expression of α_e during net evaporation/condensation (Eq. (17)) is

$$\alpha_\mathrm{e} = \beta_\mathrm{ne}(T_\mathrm{L}). \tag{22}$$

Furthermore, a general expression of α_c during net evaporation (Eq. (18)) is

$$\alpha_\mathrm{c} = \alpha_\mathrm{e} = \beta_\mathrm{ne}(T_\mathrm{L}), \tag{23}$$

and that of α_c during net condensation (Eq. (19)) is

$$\alpha_\mathrm{c} = \frac{\rho^*(T_\mathrm{L})}{\sigma}(\alpha_\mathrm{e} - \beta_\mathrm{nc}(T_\mathrm{L})) + \beta_\mathrm{nc} = \frac{\rho^*(T_\mathrm{L})}{\sigma}(\beta_\mathrm{ne}(T_\mathrm{L}) - \beta_\mathrm{nc}(T_\mathrm{L})) + \beta_\mathrm{nc}. \tag{24}$$

From Eqs. (23) and (24), we can confirm that α_e and α_c are equal to β_ne in the vapor–liquid equilibrium ($\sigma = \rho^*$).

Since we have confirmed the existence of the linear mass flux relation (Eqs. (20) and (21)) in consideration of the liquid temperature dependence, we can construct the KBCs by using the method as explained in Sec. 2.3. Substitution of Eq. (20) or (21) in Eq. (14) leads to

$$f_\mathrm{out} = \frac{\left[\beta_\mathrm{ne}(T_\mathrm{L})(\rho^*(T_\mathrm{L}) - \sigma) + \sigma\right]}{(\sqrt{2\pi R T_\mathrm{L}})^3} \exp\left(-\frac{\xi_i^2}{2RT_\mathrm{L}}\right), \quad \text{for } \xi_z > 0, \tag{25}$$

$$f_\mathrm{out} = \frac{\left[\beta_\mathrm{nc}(T_\mathrm{L})(\rho^*(T_\mathrm{L}) - \sigma) + \sigma\right]}{(\sqrt{2\pi R T_\mathrm{L}})^3} \exp\left(-\frac{\xi_i^2}{2RT_\mathrm{L}}\right), \quad \text{for } \xi_z > 0. \tag{26}$$

If the kinetic boundary is in net evaporation, we impose Eq. (25) as the KBC. Similarly, if the kinetic boundary is in net condensation, we impose Eq. (26) as the KBC. To distinguish between net evaporation and condensation, we have to examine whether the degree of net evaporation and condensation σ/ρ^* is larger of smaller than unity. It should be emphasized that the process of distinguishing net evaporation/condensation based on σ/ρ^* can be easily implemented to the algorithm to solve the Boltzmann equation because σ is a part of solution of the Boltzmann equation. Furthermore, if we consider the system that is in only net evaporation or condensation, such as cavitation bubble nucleation and shock tube experiment[47], we can make the algorithm simpler. It is important result of this study that we do not have to use the values of α_e and α_c depending on the index of the degree of net evaporation/condensation, such as the Mach number of vapor far from the interface[14, 15].

In Eqs. (25) and (26), saturated vapor density ρ^* is the function of liquid temperature, β_ne and β_nc are also the function of the liquid temperature (Fig. 4), and σ is estimated as a part of solution of the Boltzmann equation by using Eq. (4); simulating the vapor–liquid two-phase flow with net evaporation/condensation is possible if only liquid temperature is specified. Needless to say, we can impose the KBCs (Eqs. (25) and (26)) more easily than the previous ones because the liquid temperature dependence is explicitly clarified.

3.3. Validation of the constructed KBC

As a prerequisite for the validation, we confirmed whether Eqs. (25) and (26) satisfy the conditions that should be satisfied in the KBC at the vapor–liquid interface[8]. The general form of the KBC at the vapor–liquid interface is expressed in terms of a scattering kernel, K_{I}, as

$$f_{\mathrm{out}} = g_{\mathrm{I}}(\boldsymbol{x}, \boldsymbol{\xi}, t) + \int_{\tilde{\xi}_z<0} K_{\mathrm{I}}(\boldsymbol{x}, \boldsymbol{\xi}, \tilde{\boldsymbol{\xi}}, t) f_{\mathrm{coll}}(\boldsymbol{x}, \tilde{\boldsymbol{\xi}}, t) \mathrm{d}\tilde{\boldsymbol{\xi}}, \quad \text{for } \xi_z > 0, \tag{27}$$

where $\tilde{\boldsymbol{\xi}}$ denotes the molecular velocity colliding onto the interface ($\tilde{\xi}_z < 0$) and g_{I}, independent of f_{coll}, corresponds to the term including the saturated vapor density ρ^* in Eqs. (25) and (26). As for the KBC at the vapor–liquid interface, g_{I} and K_{I} are required to satisfy the following three conditions.

The first condition is that g_{I} should be non-negative function for $\xi_z > 0$. As for the constructed KBCs (Eqs. (25) and (26)), each of g_{I} is given by

$$g_{\mathrm{I}}(\boldsymbol{\xi}) = \frac{\beta_{\mathrm{ne}}(T_{\mathrm{L}})\rho^*(T_{\mathrm{L}})}{(\sqrt{2\pi R T_{\mathrm{L}}})^3} \exp\left(-\frac{\xi_i^2}{2RT_{\mathrm{L}}}\right), \tag{28}$$

$$g_{\mathrm{I}}(\boldsymbol{\xi}) = \frac{\beta_{\mathrm{nc}}(T_{\mathrm{L}})\rho^*(T_{\mathrm{L}})}{(\sqrt{2\pi R T_{\mathrm{L}}})^3} \exp\left(-\frac{\xi_i^2}{2RT_{\mathrm{L}}}\right). \tag{29}$$

where β_{ne} and β_{nc} are non-negative as shown in Figs. 3 and 4; thus, each of g_{I} is non-negative function.

The second condition is that K_{I} should be non-negative function for $\xi_z > 0$ and $\tilde{\xi}_z < 0$. As for the constructed KBCs (Eqs. (25) and (26)), each of K_{I} is given by

$$K_{\mathrm{I}}(\boldsymbol{\xi}, \tilde{\boldsymbol{\xi}}) = (1 - \beta_{\mathrm{ne}}) \frac{-1}{2\pi (RT_{\mathrm{L}})^2} \tilde{\xi}_z \exp\left(-\frac{\xi_i^2}{2RT_{\mathrm{L}}}\right), \tag{30}$$

$$K_{\mathrm{I}}(\boldsymbol{\xi}, \tilde{\boldsymbol{\xi}}) = (1 - \beta_{\mathrm{nc}}) \frac{-1}{2\pi (RT_{\mathrm{L}})^2} \tilde{\xi}_z \exp\left(-\frac{\xi_i^2}{2RT_{\mathrm{L}}}\right). \tag{31}$$

where β_{ne} and β_{nc} are smaller than unity as shown in Fig. 4; thus, each of K_{I} is non-negative function.

The third condition is that K_{I} should satisfy the following relation when the vapor–liquid equilibrium,

$$f^*_{\mathrm{out}}(\boldsymbol{\xi}) = g_{\mathrm{I}}(\boldsymbol{\xi}) + \int_{\xi_z<0} K_{\mathrm{I}}(\boldsymbol{\xi}, \tilde{\boldsymbol{\xi}}) f^*_{\mathrm{coll}}(\tilde{\boldsymbol{\xi}}) \mathrm{d}\tilde{\boldsymbol{\xi}}, \quad \text{for } \xi_z > 0, \tag{32}$$

where

$$f^*_{\mathrm{out}} = \frac{\rho^*(T_{\mathrm{L}})}{(\sqrt{2\pi R T_{\mathrm{L}}})^3} \exp\left(-\frac{\xi_i^2}{2RT_{\mathrm{L}}}\right). \tag{33}$$

Note that the sum of f^*_{out} and f^*_{coll} is equal to the equilibrium solution of the Boltzmann equation; that is the Maxwellian distribution. Eqs. (32) and (33) are the result of the local property of K_{I}, and the natural requirement that the vapor–liquid equilibrium at liquid temperature T_{L} and saturated vapor density at liquid temperature $\rho^*(T_{\mathrm{L}})$ is established in

the system. As for the constructed KBCs (Eqs. (25) and (26)), σ is equal to ρ^* in the vapor–liquid equilibrium; therefore, Eqs. (25) and (26) becomes Eq. (33). On the basis of the above discussion, we confirmed that the constructed KBCs (Eqs (25) and (26)) satisfy the conditions that should be satisfied in the KBC at the vapor–liquid interface.

Then, to validate the accuracy of the constructed KBCs (Eqs. (25) and (26)), we compared the macroscopic variables, such as vapor velocity and temperature, obtained from the numerical simulation of the Boltzmann equation and those obtained from the EV-DSMC simulation. The macroscopic variables in vapor strongly depend on the KBC; hence, the KBC is validated if and only if the macroscopic variables obtained from these two simulations agree with the high degree of accuracy. Note that the validation method same as this study has been performed based on molecular dynamics[46].

In the simulation of the Boltzmann equation, we considered a one-dimensional physical space (z-direction) and three-dimensional molecular velocity space in the system that is composed of hard-sphere vapor between two boundaries; one of the boundaries is the vapor–liquid interface (kinetic boundary), and the other is an arbitrary vapor boundary. At the kinetic boundary, we prescribed the constructed KBC (Eqs. (25) or (26)), while at the vapor boundary, we prescribed the velocity distribution function, f_{VB}, as follows:

$$f_{\mathrm{VB}} = \frac{\nu\rho^*(T_{\mathrm{L}})}{(\sqrt{2\pi R\nu T_{\mathrm{L}}})^3} \exp\left(-\frac{\xi_i^2}{2R\nu T_{\mathrm{L}}}\right) \quad \text{for } \xi_z < 0, \tag{34}$$

where ν is a constant parameter ($\nu > 0$) and is set at 0.5 and 1.5. The system is in net evaporation in the case of $\nu = 0.5$, while that is in net condensation in the case of $\nu = 1.5$. To set the Prandtl number of hard-sphere molecules as 0.66[8], we utilize the ES-BGK model Boltzmann equation (ES-BGK equation)[48] which is one of the models of the Boltzmann equation. The finite difference method is used for the numerical scheme. After the velocity distribution function f in vapor is obtained from the numerical simulation of the ES-BGK equation, the macroscopic variables, such as vapor velocity and temperature, are estimated by Eq. (1). A more detailed explanation of the ES-BGK equation and the numerical scheme can be found in the literature[48, 49].

In the EV-DSMC simulation, we considered a one-dimensional physical space (z-direction) and three-dimensional molecular velocity space in the system that is composed of hard-sphere vapor and its condensed phase (liquid). A schematic of this simulation is shown in Fig. 5 (above). We prescribed Eq. (34) at the vapor boundary in the same way as the simulation of the ES-BGK equation. The cell and time-step sizes are the same as already explained in Sec. 2.3. Since the liquid slab deminishes/grows due to net evaporation/condensation, we utilized a *sampling window* (Fig. 5 (above)) which moves in accordance with following coordinate, z'':

$$z'' = z - \frac{\rho v_z}{\rho_{\mathrm{L}}} t, \tag{35}$$

where ρ_{L} is liquid density. Note that in this simulation settings, the length between the right end of the sampling window and system end, Z_{e}, is smaller than the mean free path of hard-sphere molecules. Thus, we can regard the velocity distribution function at the right end of the sampling window as Eq. (34).

Figure 5 (below) shows the comparison between the vapor velocity and temperature fields obtained from the numerical simulation of the ES-BGK equation and the EV-DSMC simulation, where dashed lines are the results of the ES-BGK equation, and solid lines are those of the EV-DSMC simulation. As can be observed, in the case of $T_{\rm L}/T_{\rm c} = 0.60$ (Fig. 5(a) and 5(b)), the vapor velocity and temperature fields obtained from the numerical simulation of the ES-BGK equation and the EV-DSMC simulation are in excellent agreement. In the case of $T_{\rm L}/T_{\rm c} = 0.68$ (Fig. 5(c) and 5(d)), these macroscopic variables are also in excellent agreement except for the vapor temperature fields in the vicinity of the kinetic boundary during net evaporation (Fig. 5(d)); however, the maximum deviation of the vapor temperature fields obtained from these two simulations is less than 5%. Based on these results, we conclude that the deviation of the macroscopic variables obtained from these two simulations is sufficiently small; hence, the KBC constructed in this study is guaranteed to be accurate.

3.4. Application for the fluid-dynamic-type equations

With the use of the constructed KBCs (Eqs. (25) and (26)), we can derive the boundary conditions during net evaporation and condensation for the fluid-dynamic-type equations; the derivation is shown in the literature[8, 40, 50]. The boundary conditions of vapor pressure, p, and temperature, T, during net evaporation ($v_z > 0$) are as follows:

$$\begin{aligned} \frac{p - p^*(T_{\rm L})}{p^*(T_{\rm L})} &= \left(C_4^* - 2\sqrt{\pi} \frac{1 - \beta_{\rm ne}(T_{\rm L})}{\beta_{\rm ne}(T_{\rm L})} \right) \frac{v_z}{\sqrt{2RT_{\rm L}}}, \\ \frac{T - T_{\rm L}}{T_{\rm L}} &= d_4^* \frac{v_z}{\sqrt{2RT_{\rm L}}}, \end{aligned} \tag{36}$$

where p^* is the saturated vapor pressure, and C_4^* and d_4^* are the slip coefficients determined by specifying the molecular model[8]. Similarly, that for net condensation ($v_z < 0$) is as follows:

$$\begin{aligned} \frac{p - p^*}{p^*} &= \left(C_4^* - 2\sqrt{\pi} \frac{1 - \beta_{\rm nc}(T_{\rm L})}{\beta_{\rm nc}(T_{\rm L})} \right) \frac{v_z}{\sqrt{2RT_{\rm L}}}, \\ \frac{T - T_{\rm L}}{T_{\rm L}} &= d_4^* \frac{v_z}{\sqrt{2RT_{\rm L}}}. \end{aligned} \tag{37}$$

It should be emphasized that $\beta_{\rm ne}$ and $\beta_{\rm nc}$ are functions of liquid temperature as shown in Fig. 4; thus, we can determine the boundary conditions for the fluid-dynamic-type equations by simply specifying liquid temperature. This enables us to deal with a larger spatio-temporal scale of interfacial dynamics in the vapor–liquid two-phase system with net evaporation/condensation, such as Leidenfrost effect[1, 2, 3] and cavitation bubble collapse[4, 5, 6].

4. Conclusion

In this paper, we conducted a systematic investigation of the kinetic boundary condition (KBC) for hard–sphere molecules during steady net evaporation/condensation over a wide

range of liquid temperature. First, we constructed the KBC in the case of the normalized liquid temperature, $T_{\mathrm{L}}/T_{\mathrm{c}}$, from 0.60 to 0.72 by the numerical simulation based on mean field kinetic theory. The results showed that the parameters including in the KBCs, β_{ne} and β_{nc}, to be constants at each liquid temperature; thus, we can prescribe the KBCs during net evaporation/condensation by simply specifying liquid temperature. Then, we validated the constructed KBC by comparing the macroscopic variables in vapor obtained from molecular gas dynamics and mean field kinetic theory. The macroscopic variables in vapor obtained from these theories agree with the high degree of accuracy, indicating that the constructed KBC can be guaranteed to be accurate for the analysis of vapor–liquid two-phase system with net evaporation/condensation. Finally, to deal with a large spatio-temporal scale of interfacial dynamics, we discussed the application of the constructed KBC to the boundary condition for the fluid-dynamic-type equations.

On the based on the results of this study, we constructed the KBC for hard-sphere molecules in consideration of the liquid temperature dependence during steady net evaporation and condensation; however, the application of the KBC during unsteady net evaporation/condensation is extremely important. In general, the unsteady molecular simulation requires the larger number of samples than the steady one. In contrast, we can probably simulate the unsteady problem precisely by using the EV-DSMC simulation. Furthermore, we now need to estimate β_{ne} and β_{nc} for other substances, such as water, to construct a KBC of more practical use. The values of evaporation and condensation coefficients of water is proposed from 10^{-3} up to 1[51]. On the other hand, our previous experimental study[47] has proposed that a linear mass flux relation exists for water and methanol, implying that β_{ne} and β_{nc} for other substance can be determined in accordance with this study by adopting a more practical potential, namely Lennard–Jones intermolecular potential. The investigation of the liquid temperature dependence of β_{ne} and β_{nc} for other substances remains a subject for future work.

5. Acknowledgement

This study was partly supported by JSPS Grant-in-Aid for Young Scientists (B) (25820038).

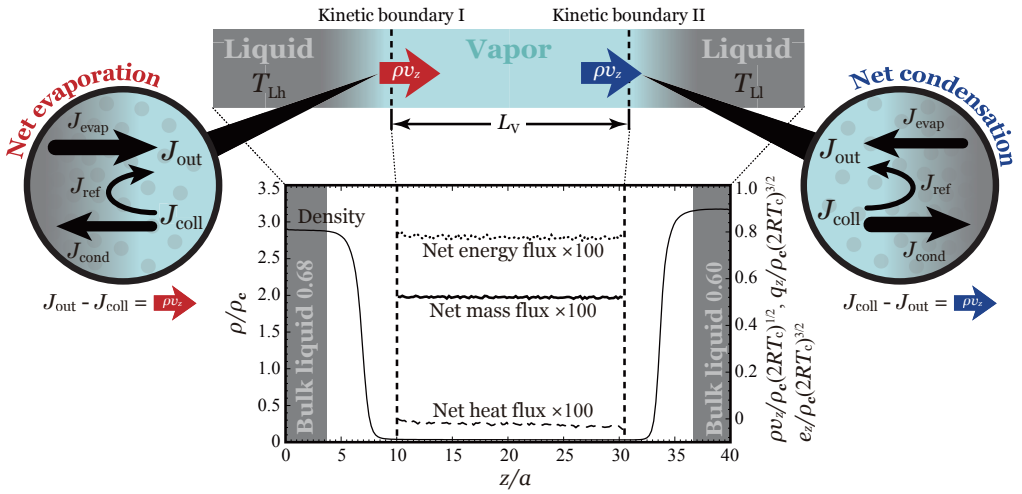

Figure 1: (above) Schematic of the simulation system for constructing the KBC and the mass flux relations at each kinetic boundary. (below) Density field, ρ, the net mass flux, ρv_z, the net heat flux, q_z, and the net energy flux, e_z, obtained from the EV-DSMC simulation at $T_{Lh}/T_c = 0.68$ and $T_{Ll}/T_c = 0.60$; the abscissa is normalized by the molecular diameter, a, and each ordinate is normalized by its critical values, ρ_c and T_c.

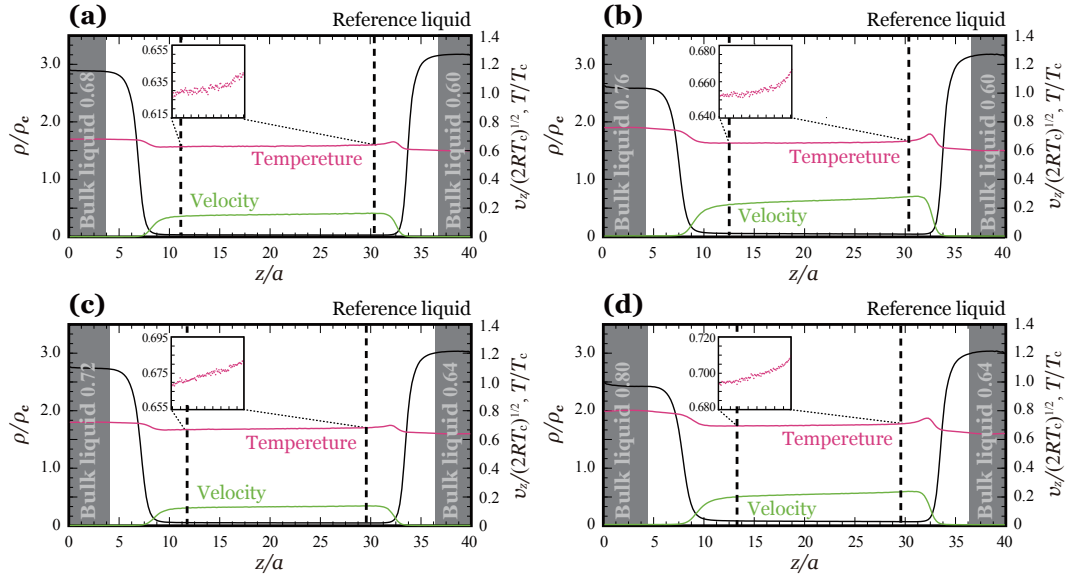

Figure 2: Density, ρ, velocity, v_z, and temperature, T, fields obtained from the EV-DSMC method in the cases of $T_L/T_c = 0.60$ and 0.64: (a) $T_{Lh}/T_c = 0.68$ and $T_{Ll}/T_c = 0.60$ ($T_L/T_c = 0.60$), (b) $T_{Lh}/T_c = 0.76$ and $T_{Ll}/T_c = 0.60$ ($T_L/T_c = 0.60$), (c) $T_{Lh}/T_c = 0.72$ and $T_{Ll}/T_c = 0.64$ ($T_L/T_c = 0.64$), and (d) $T_{Lh}/T_c = 0.80$ and $T_{Ll}/T_c = 0.64$ ($T_L/T_c = 0.64$); the abscissa is normalized by the molecular diameter, a, and each ordinate is normalized by its critical values, ρ_c and T_c.

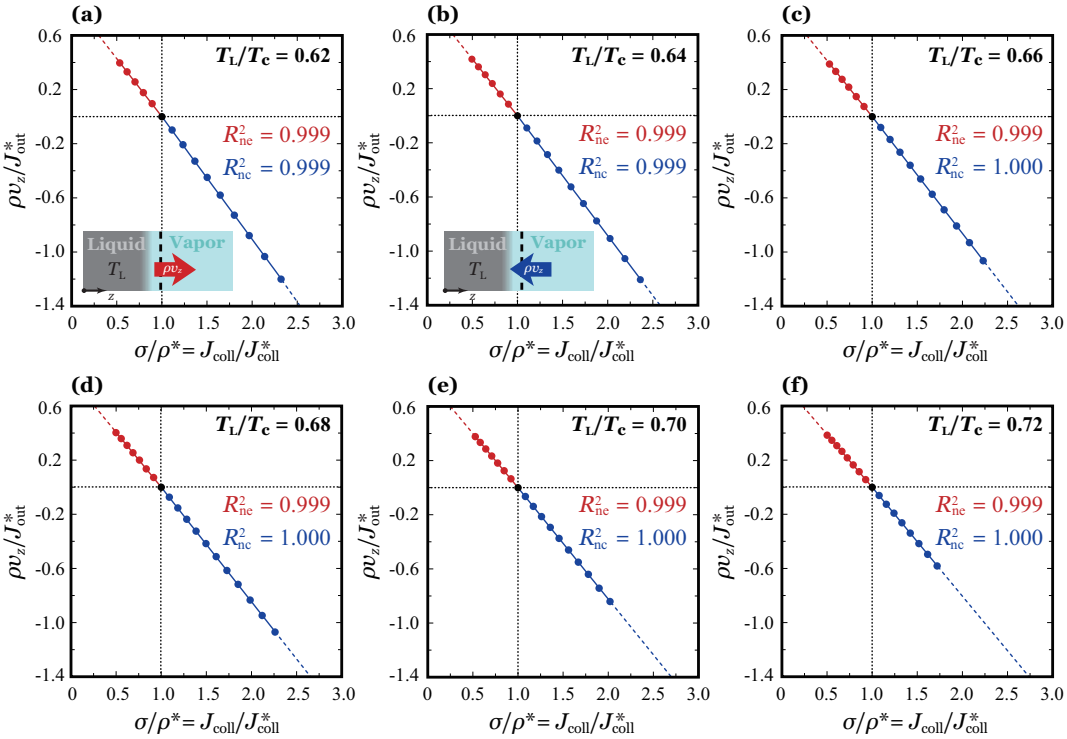

Figure 3: Mass flux relation between the net mass flux, ρv_z, and the degree of net evaporation/condensation, σ/ρ^*, at each reference liquid temperature: (a) $T_L/T_c = 0.62$, (b) $T_L/T_c = 0.64$, (c) $T_L/T_c = 0.66$, (d) $T_L/T_c = 0.68$, (e) $T_L/T_c = 0.70$, and (f) $T_L/T_c = 0.72$; the ordinate is normalized by the molecular mass flux outgoing from the liquid into the vapor phase in the vapor–liquid equilibrium, J^*_{out}.

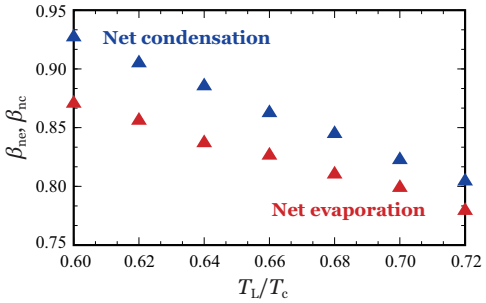

Figure 4: Liquid temperature dependence of β_{ne} and β_{nc}; the abscissa is normalized by its critical value, T_c.

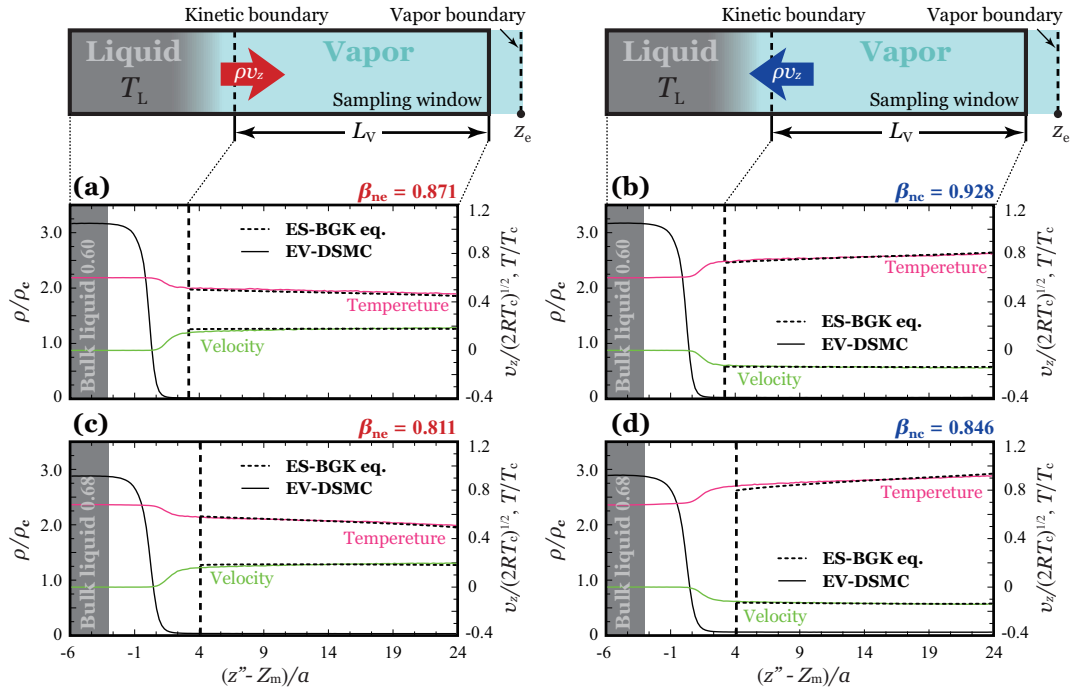

Figure 5: (above) Schematic of simulation system for validating the constructed KBC. (below) Comparison of the velocity, v_z, and temperature, T, fields in vapor obtained from the EV-DSMC simulation and the numerical simulation of the ES-BGK equation: (a) $T_L/T_c = 0.60$ and $nu = 0.5$, (b) $T_L/T_c = 0.68$ and $\nu = 0.5$, (c) $T_L/T_c = 0.60$ and $\nu = 1.5$, and (d) $T_L/T_c = 0.68$ and $\nu = 1.5$; the abscissa is normalized by the molecular diameter, a, and each ordinates is normalized by its critical values, ρ_c and T_c.

Table 1: Results of the EV-DSMC simulation at $T_{\mathrm{L}}/T_{\mathrm{c}} = 0.60$.

#	$T_{\mathrm{Lh}}/T_{\mathrm{c}}$	$T_{\mathrm{Ll}}/T_{\mathrm{c}}$	L_{V}/a	$\rho v_z/J^*_{\mathrm{out}}$	σ/ρ^*	β_{ne}	β_{nc}
1	0.60	0.56	21.2	0.3607	0.5849		—
2	0.60	0.57	21.0	0.2821	0.6773	0.871	—
3	0.60	0.58	20.8	0.1934	0.7782		—
4	0.60	0.59	20.8	0.1014	0.8848		—
5	0.61	0.60	20.4	-0.1086	1.1265	—	
6	0.62	0.60	20.4	-0.2376	1.2561	—	
7	0.63	0.60	20.2	-0.3696	1.4021	—	
8	0.64	0.60	20.0	-0.5069	1.5526	—	0.927
9	0.65	0.60	19.8	-0.6595	1.7157	—	
10	0.66	0.60	19.8	-0.8262	1.8909	—	
11	0.67	0.60	19.6	-0.9988	2.0747	—	
12	0.68	0.60	19.4	-1.1863	2.2715	—	
13	0.69	0.60	19.2	-1.3910	2.4828	—	—
14	0.70	0.60	19.0	-1.5897	2.6969	—	—
15	0.71	0.60	18.8	-1.8177	2.9321	—	—
16	0.72	0.60	18.6	-2.0326	3.1667	—	—
17	0.73	0.60	18.4	-2.2806	3.4248	—	—
18	0.74	0.60	18.2	-2.5354	3.6930	—	—
19	0.75	0.60	18.0	-2.8078	3.9771	—	—
20	0.76	0.60	17.8	-3.0871	4.2714	—	—

Table 2: Results of the EV-DSMC simulation at $T_{\mathrm{L}}/T_{\mathrm{c}} = 0.62$.

#	$T_{\mathrm{Lh}}/T_{\mathrm{c}}$	$T_{\mathrm{Ll}}/T_{\mathrm{c}}$	L_{V}/a	$\rho v_z/J^*_{\mathrm{out}}$	σ/ρ^*	β_{ne}	β_{nc}
21	0.62	0.56	21.0	0.4530	0.4616	—	—
22	0.62	0.57	20.8	0.3969	0.5342		—
23	0.62	0.58	20.6	0.3313	0.6141		—
24	0.62	0.59	20.6	0.2567	0.7015	0.857	—
25	0.62	0.60	20.4	0.1770	0.7946		—
26	0.62	0.61	20.2	0.0955	0.8922		—
27	0.63	0.62	20.0	-0.0990	1.1129	—	
28	0.64	0.62	19.8	-0.2068	1.2340	—	
29	0.65	0.62	19.8	-0.3282	1.3656	—	
30	0.66	0.62	19.6	-0.4490	1.5013	—	
31	0.67	0.62	19.4	-0.5800	1.6464	—	0.906
32	0.68	0.62	19.2	-0.7273	1.8039	—	
33	0.69	0.62	19.0	-0.8780	1.9678	—	
34	0.70	0.62	18.8	-1.0339	2.1391	—	
35	0.71	0.62	18.6	-1.2006	2.3207	—	
36	0.72	0.62	18.4	-1.3852	2.5164	—	—
37	0.73	0.62	18.2	-1.5613	2.7127	—	—
38	0.74	0.62	18.0	-1.7614	2.9267	—	—
39	0.75	0.62	17.8	-1.9713	3.1510	—	—
40	0.76	0.62	17.6	-2.1833	3.3819	—	—

Table 3: Results of the EV-DSMC simulation at $T_{\mathrm{L}}/T_{\mathrm{c}} = 0.64$.

#	$T_{\mathrm{Lh}}/T_{\mathrm{c}}$	$T_{\mathrm{Ll}}/T_{\mathrm{c}}$	L_{V}/a	$\rho v_z/J^*_{\mathrm{out}}$	σ/ρ^*	β_{ne}	β_{nc}
41	0.64	0.56	20.6	0.5147	0.3707	—	—
42	0.64	0.57	20.4	0.4716	0.4300	—	—
43	0.64	0.58	20.2	0.4183	0.4963		—
44	0.64	0.59	20.2	0.3613	0.5670		—
45	0.64	0.60	20.0	0.3021	0.6416	0.838	—
46	0.64	0.61	19.8	0.2378	0.7214		—
47	0.64	0.62	19.8	0.1611	0.8098		—
48	0.64	0.63	19.6	0.0860	0.9008		—
49	0.65	0.64	19.4	-0.0903	1.1043	—	
50	0.66	0.64	19.2	-0.1872	1.2153	—	
51	0.67	0.64	19.0	-0.2875	1.3314	—	
52	0.68	0.64	18.8	-0.4024	1.4583	—	
53	0.69	0.64	18.6	-0.5257	1.5930	—	0.886
54	0.70	0.64	18.4	-0.6492	1.7318	—	
55	0.71	0.64	18.2	-0.7771	1.8768	—	
56	0.72	0.64	18.0	-0.9069	2.0268	—	
57	0.73	0.64	17.8	-1.0556	2.1903	—	
58	0.74	0.64	17.6	-1.2116	2.3618	—	
59	0.75	0.64	17.4	-1.3700	2.5389	—	—
60	0.76	0.64	17.2	-1.5420	2.7273	—	—
61	0.77	0.64	17.0	-1.7076	2.9158	—	—
62	0.78	0.64	16.8	-1.8916	3.1216	—	—
63	0.79	0.64	16.6	-2.0797	3.3328	—	—
64	0.80	0.64	16.4	-2.2865	3.5559	—	—

Table 4: Results of the EV-DSMC simulation at $T_{\mathrm{L}}/T_{\mathrm{c}} = 0.66$.

#	$T_{\mathrm{Lh}}/T_{\mathrm{c}}$	$T_{\mathrm{Ll}}/T_{\mathrm{c}}$	L_{V}/a	$\rho v_z/J^*_{\mathrm{out}}$	σ/ρ^*	β_{ne}	β_{nc}
65	0.66	0.56	20.4	0.5587	0.3021	—	—
66	0.66	0.57	20.2	0.5219	0.3525	—	—
67	0.66	0.58	20.0	0.4822	0.4064	—	—
68	0.66	0.59	20.0	0.4343	0.4661	—	—
69	0.66	0.60	19.8	0.3889	0.5271		—
70	0.66	0.61	19.6	0.3348	0.5944		—
71	0.66	0.62	19.6	0.2765	0.6661	0.827	—
72	0.66	0.63	19.4	0.2181	0.7406		—
73	0.66	0.64	19.2	0.1480	0.8229		—
74	0.66	0.65	19.0	0.0757	0.9092		—
75	0.67	0.66	18.8	-0.0799	1.0955	—	
76	0.68	0.66	18.6	-0.1687	1.1982	—	
77	0.69	0.66	18.4	-0.2632	1.3067	—	
78	0.70	0.66	18.2	-0.3588	1.4191	—	
79	0.71	0.66	18.0	-0.4603	1.5375	—	0.863
80	0.72	0.66	17.8	-0.5728	1.6647	—	
81	0.73	0.66	17.6	-0.6879	1.7966	—	
82	0.74	0.66	17.4	-0.8071	1.9341	—	
83	0.75	0.66	17.2	-0.9313	2.0776	—	
84	0.76	0.66	17.0	-1.0640	2.2290	—	
85	0.77	0.66	16.8	-1.2030	2.3873	—	—
86	0.78	0.66	16.6	-1.3473	2.5521	—	—
87	0.79	0.66	16.4	-1.5018	2.7259	—	—
88	0.80	0.66	16.2	-1.6550	2.9029	—	—

Table 5: Results of the EV-DSMC simulation at $T_{\mathrm{L}}/T_{\mathrm{c}} = 0.68$.

#	$T_{\mathrm{Lh}}/T_{\mathrm{c}}$	$T_{\mathrm{Ll}}/T_{\mathrm{c}}$	L_{V}/a	$\rho v_z/J^*_{\mathrm{out}}$	σ/ρ^*	β_{ne}	β_{nc}
89	0.68	0.56	20.0	0.5854	0.2513	—	—
90	0.68	0.57	19.8	0.5558	0.2938	—	—
91	0.68	0.58	19.6	0.5234	0.3393	—	—
92	0.68	0.59	19.6	0.4887	0.3878	—	—
93	0.68	0.60	19.4	0.4486	0.4405	—	—
94	0.68	0.61	19.4	0.4038	0.4974		—
95	0.68	0.62	19.2	0.3593	0.5563		—
96	0.68	0.63	19.0	0.3094	0.6198		—
97	0.68	0.64	18.8	0.2553	0.6874	0.811	—
98	0.68	0.65	18.6	0.1996	0.7581		—
99	0.68	0.66	18.6	0.1354	0.8352		—
100	0.68	0.67	18.4	0.0715	0.9146		—
101	0.69	0.68	18.0	-0.0745	1.0893	—	
102	0.70	0.68	17.8	-0.1535	1.1834	—	
103	0.71	0.68	17.6	-0.2360	1.2820	—	
104	0.72	0.68	17.4	-0.3254	1.3867	—	
105	0.73	0.68	17.2	-0.4166	1.4951	—	
106	0.74	0.68	17.0	-0.5126	1.6088	—	0.846
107	0.75	0.68	16.8	-0.6156	1.7289	—	
108	0.76	0.68	16.6	-0.7177	1.8516	—	
109	0.77	0.68	16.4	-0.8337	1.9842	—	
110	0.78	0.68	16.2	-0.9470	2.1187	—	
111	0.79	0.68	16.0	-1.0699	2.2612	—	
112	0.80	0.68	15.8	-1.1912	2.4062	—	—

Table 6: Results of the EV-DSMC simulation at $T_{\mathrm{L}}/T_{\mathrm{c}} = 0.70$.

#	$T_{\mathrm{Lh}}/T_{\mathrm{c}}$	$T_{\mathrm{Ll}}/T_{\mathrm{c}}$	L_{V}/a	$\rho v_z/J^*_{\mathrm{out}}$	σ/ρ^*	β_{ne}	β_{nc}
113	0.70	0.56	19.6	0.5985	0.2142	—	—
114	0.70	0.57	19.4	0.5746	0.2503	—	—
115	0.70	0.58	19.2	0.5465	0.2897	—	—
116	0.70	0.59	19.0	0.5172	0.3313	—	—
117	0.70	0.60	19.0	0.4886	0.3746	—	—
118	0.70	0.61	18.8	0.4523	0.4225	—	—
119	0.70	0.62	18.8	0.4152	0.4729	—	—
120	0.70	0.63	18.6	0.3770	0.5255		—
121	0.70	0.64	18.4	0.3348	0.5818		—
122	0.70	0.65	18.2	0.2861	0.6429		—
123	0.70	0.66	18.2	0.2340	0.7076	0.800	—
124	0.70	0.67	18.2	0.1820	0.7745		—
125	0.70	0.68	17.8	0.1247	0.8458		—
126	0.70	0.69	17.6	0.0654	0.9204		—
127	0.71	0.70	17.2	-0.0656	1.0820	—	
128	0.72	0.70	17.0	-0.1386	1.1696	—	
129	0.73	0.70	16.8	-0.2134	1.2607	—	
130	0.74	0.70	16.6	-0.2928	1.3564	—	
131	0.75	0.70	16.4	-0.3752	1.4561	—	
132	0.76	0.70	16.2	-0.4600	1.5595	—	0.823
133	0.77	0.70	16.0	-0.5496	1.6679	—	
134	0.78	0.70	15.8	-0.6406	1.7796	—	
135	0.79	0.70	15.6	-0.7422	1.8992	—	
136	0.80	0.70	15.4	-0.8414	2.0203	—	

Table 7: Results of the EV-DSMC simulation at $T_{\mathrm{L}}/T_{\mathrm{c}} = 0.72$.

#	$T_{\mathrm{Lh}}/T_{\mathrm{c}}$	$T_{\mathrm{Ll}}/T_{\mathrm{c}}$	L_{V}/a	$\rho v_z/J^*_{\mathrm{out}}$	σ/ρ^*	β_{ne}	β_{nc}
137	0.72	0.56	19.2	0.6066	0.1855	—	—
138	0.72	0.57	19.0	0.5872	0.2165	—	—
139	0.72	0.58	18.8	0.5654	0.2499	—	—
140	0.72	0.59	18.6	0.5428	0.2850	—	—
141	0.72	0.60	18.6	0.5151	0.3237	—	—
142	0.72	0.61	18.4	0.4872	0.3640	—	—
143	0.72	0.62	18.4	0.4575	0.4068	—	—
144	0.72	0.63	18.2	0.4228	0.4531	—	—
145	0.72	0.64	18.0	0.3847	0.5025		—
146	0.72	0.65	17.8	0.3472	0.5535		—
147	0.72	0.66	17.8	0.3063	0.6078		—
148	0.72	0.67	17.6	0.2647	0.6642	0.780	—
149	0.72	0.68	17.4	0.2175	0.7248		—
150	0.72	0.69	17.2	0.1648	0.7898		—
151	0.72	0.70	17.0	0.1140	0.8560		—
152	0.72	0.71	16.8	0.0566	0.9271		—
153	0.73	0.72	16.4	-0.0613	1.0769	—	
154	0.74	0.72	16.2	-0.1261	1.1577	—	
155	0.75	0.72	16.0	-0.1914	1.2408	—	
156	0.76	0.72	15.8	-0.2631	1.3291	—	0.805
157	0.77	0.72	15.6	-0.3392	1.4217	—	
158	0.78	0.72	15.4	-0.4167	1.5173	—	
159	0.79	0.72	15.2	-0.4966	1.6163	—	
160	0.80	0.72	15.0	-0.5816	1.7201	—	

References

[1] J. G. Leidenfrost, On the fixation of water in diverse fire, International Journal of Heat and Mass Transfer 9 (11) (1966) 1153–1166.

[2] H. Linke, B. Alemán, L. Melling, M. Taormina, M. Francis, C. Dow-Hygelund, V. Narayanan, R. Taylor, A. Stout, Self-propelled leidenfrost droplets, Physical Review Letters 96 (15) (2006) 154502.

[3] D. Quéré, Leidenfrost dynamics, Annual Review of Fluid Mechanics 45 (2013) 197–215.

[4] S. Fujikawa, T. Akamatsu, Effects of the non-equilibrium condensation of vapour on the pressure wave produced by the collapse of a bubble in a liquid, Journal of Fluid Mechanics 97 (03) (1980) 481–512.

[5] I. Akhatov, O. Lindau, A. Topolnikov, R. Mettin, N. Vakhitova, W. Lauterborn, Collapse and rebound of a laser-induced cavitation bubble, Physics of Fluids 13 (10) (2001) 2805–2819.

[6] Y. Jinbo, T. Ogasawara, H. Takahira, Influence of the nonequilibrium phase transition on the collapse of inertia nonspherical bubbles in a compressible liquid, Experimental Thermal and Fluid Science 60 (2015) 374–384.

[7] J. Lee, T. Laoui, R. Karnik, Nanofluidic transport governed by the liquid/vapour interface, Nature Nanotechnology 9 (4) (2014) 317–323.

[8] Y. Sone, Molecular gas dynamics: theory, techniques, and applications, Springer Science & Business Media, 2007.

[9] R. Meland, T. Ytrehus, Dependence of the inverted temperature gradient phenomenon on the condensation coefficient, Physics of Fluids 16 (3) (2004) 836–838.

[10] M. Matsumoto, Molecular dynamics of fluid phase change, Fluid Phase Equilibria 144 (1) (1998) 307–314.

[11] T. Tsuruta, H. Tanaka, T. Masuoka, Condensation/evaporation coefficient and velocity distributions at liquid–vapor interface, International Journal of Heat and Mass Transfer 42 (22) (1999) 4107–4116.

[12] T. Ishiyama, T. Yano, S. Fujikawa, Molecular dynamics study of kinetic boundary condition at an interface between argon vapor and its condensed phase, Physics of Fluids 16 (8) (2004) 2899–2906.

[13] M. Bond, H. Struchtrup, Mean evaporation and condensation coefficients based on energy dependent condensation probability, Physical Review E 70 (6) (2004) 061605.

[14] K. Gu, C. B. Watkins, J. Koplik, Multiscale molecular simulations of argon vapor condensation onto a cooled substrate with bulk flow, Physics of Fluids 22 (11) (2010) 112002.

[15] R. Meland, A. Frezzotti, T. Ytrehus, B. Hafskjold, Nonequilibrium molecular-dynamics simulation of net evaporation and net condensation, and evaluation of the gas-kinetic boundary condition at the interphase, Physics of Fluids 16 (2) (2004) 223–243.

[16] A. Kryukov, V. Y. Levashov, About evaporation–condensation coefficients on the vapor–liquid interface of high thermal conductivity matters, International Journal of Heat and Mass Transfer 54 (13) (2011) 3042–3048.

[17] K. Gu, C. B. Watkins, J. Koplik, Molecular dynamics simulation of the equilibrium liquid–vapor interphase with solidification, Fluid Phase Equilibria 297 (1) (2010) 77–89.

[18] K. Kobayashi, K. Hori, H. Yaguchi, M. Watanabe, Molecular dynamics simulation on evaporation molecules in a vapor-liquid equilibrium state, in: AIP Conference Proceedings, Vol. 1628, AIP Publishing, 2014, pp. 404–410.

[19] T. Ishiyama, T. Yano, S. Fujikawa, Kinetic boundary condition at a vapor-liquid interface, Physical Review Letters 95 (8) (2005) 084504.

[20] T. Ishiyama, S. Fujikawa, T. Kurz, W. Lauterborn, Nonequilibrium kinetic boundary condition at the vapor-liquid interface of argon, Physical Review E 88 (4) (2013) 042406.

[21] M. Kon, K. Kobayashi, M. Watanabe, Method of determining kinetic boundary conditions in net evaporation/condensation, Physics of Fluids 26 (7) (2014) 072003.

[22] M. Grmela, Kinetic equation approach to phase transitions, Journal of Statistical Physics 3 (3) (1971) 347–364.

[23] J. Karkheck, G. Stell, Kinetic mean-field theories, The Journal of Chemical Physics 75 (3) (1981) 1475–1487.

[24] A. Frezzotti, L. Gibelli, S. Lorenzani, Mean field kinetic theory description of evaporation of a fluid into vacuum, Physics of Fluids 17 (1) (2005) 012102.
[25] N. F. Carnahan, K. E. Starling, Equation of state for nonattracting rigid spheres, The Journal of Chemical Physics 51 (2) (1969) 635–636.
[26] A. Frezzotti, A particle scheme for the numerical solution of the Enskog equation, Physics of Fluids 9 (5) (1997) 1329–1335.
[27] G. A. Bird, Molecular gas dynamics and the direct simulation of gas flows, Clarendon, 1994.
[28] K. Nanbu, Direct simulation scheme derived from the Boltzmann equation. I. Monocomponent gases, Journal of the Physical Society of Japan 49 (5) (1980) 2042–2049.
[29] P. Barbante, A. Frezzotti, L. Gibelli, A kinetic theory description of liquid menisci at the microscale, Kinetic and Related Models 8 (2) (2015) 235–254.
[30] K. Kobayashi, K. Ohashi, M. Watanabe, Numerical analysis of vapor-liquid two-phase system based on the Enskog-Vlasov equation, in: AIP Conference Proceedings, Vol. 1501, AIP Publishing, 2012, pp. 1145–1151.
[31] A. Frezzotti, M. Rossi, Slip effects at the vapor-liquid boundary, in: AIP Conference Proceedings, Vol. 1501, AIP Publishing, 2012, pp. 903–910.
[32] M. Kon, K. Kobayashi, M. Watanabe, Numerical analysis of kinetic boundary conditions at net evaporation/condensation interfaces in various liquid temperatures based on mean-field kinetic theory, in: AIP Conference Proceedings, Vol. 1628, AIP Publishing, 2014, pp. 398–403.
[33] Y. Onishi, On the negative mass flows in evaporation and condensation problems, Physics of Fluids 17 (12) (2005) 127106.
[34] H. Struchtrup, S. Kjelstrup, D. Bedeaux, Temperature-difference-driven mass transfer through the vapor from a cold to a warm liquid, Physical Review E 85 (6) (2012) 061201.
[35] H. Struchtrup, S. Kjelstrup, D. Bedeaux, Analysis of temperature difference driven heat and mass transfer in the Phillips–Onsager cell, International Journal of Heat and Mass Transfer 58 (1) (2013) 521–531.
[36] R. Meland, Molecular dynamics simulation of the inverted temperature gradient phenomenon, Physics of Fluids 15 (10) (2003) 3244–3247.
[37] G. Fang, C. Ward, Temperature measured close to the interface of an evaporating liquid, Physical Review E 59 (1) (1999) 417–428.
[38] R. Hołyst, M. Litniewski, Heat transfer at the nanoscale: evaporation of nanodroplets, Physical Review Letters 100 (5) (2008) 055701.
[39] S. Cheng, J. B. Lechman, S. J. Plimpton, G. S. Grest, Evaporation of Lennard-Jones fluids, The Journal of Chemical Physics 134 (22) (2011) 224704.
[40] Y. Sone, Y. Onishi, Kinetic theory of evaporation and condensation–Hydrodynamic equation and slip boundary condition–, Journal of the Physical Society of Japan 44 (6) (1978) 1981–1994.
[41] Y.-P. Pao, Application of kinetic theory to the problem of evaporation and condensation, Physics of Fluids 14 (2) (1971) 306–312.
[42] L. Koffman, M. Plesset, L. Lees, Theory of evaporation and condensation, Physics of Fluids 27 (4) (1984) 876–880.
[43] C. Cercignani, W. Fiszdon, A. Frezzotti, The paradox of the inverted temperature profiles between an evaporating and a condensing surface, Physics of Fluids 28 (11) (1985) 3237–3240.
[44] L. Hermans, J. Beenakker, The temperature paradox in the kinetic theory of evaporation, Physics of Fluids 29 (12) (1986) 4231–4232.
[45] C. T. Mills, L. F. Phillips, The gas–liquid interface and the paradox of inverted temperature profiles in the two-surface problem, Chemical Physics Letters 372 (5) (2003) 609–614.
[46] A. Frezzotti, P. Grosfils, S. Toxvaerd, Evidence of an inverted temperature gradient during evaporation/condensation of a Lennard-Jones fluid, Physics of Fluids 15 (10) (2003) 2837–2842.
[47] K. Kobayashi, S. Watanabe, D. Yamano, T. Yano, S. Fujikawa, Condensation coefficient of water in a weak condensation state, Fluid Dynamics Research 40 (7) (2008) 585–596.
[48] P. Andries, P. L. Tallec, J.-P. Perlat, B. Perthame, The Gaussian-BGK model of Boltzmann equation

with small prandtl number, European Journal of Mechanics - B/Fluids 19 (6) (2000) 813–830.
[49] C. Chu, Kinetic-theoretic description of shock wave formation. II., Physics of Fluids 8 (8) (1965) 1450–1455.
[50] S. Fujikawa, T. Yano, M. Watanabe, Vapor-liquid interfaces, bubbles and droplets: Fundamentals and applications, Springer Science & Business Media, 2011.
[51] R. Marek, J. Straub, Analysis of the evaporation coefficient and the condensation coefficient of water, International Journal of Heat and Mass Transfer 44 (1) (2001) 39–53.